nature photonics

ARTICLES

PUBLISHED ONLINE: 21 DECEMBER 2015 | DOI: 10.1038/NPHOTON.2015.243

Laser cooling of organic–inorganic lead halide perovskites

Son-Tung Ha[1], Chao Shen[1†], Jun Zhang[1†] and Qihua Xiong[1,2*]

Optical irradiation with suitable energy can cool solids, a phenomenon known as optical refrigeration, first proposed in 1929 and experimentally achieved in ytterbium-doped glasses in 1995. Since then, considerable progress has been made in various rare earth element-doped materials, with a recent record of cooling to 91 K directly from ambient temperatures. For practical use and to suit future applications of optical refrigeration, the discovery of materials with facile and scalable synthesis and high cooling power density will be required. Herein we present the realization of a net cooling of 23.0 K in micrometre-thick 3D $CH_3NH_3PbI_3$ ($MAPbI_3$) and 58.7 K in exfoliated 2D $(C_6H_5C_2H_4NH_3)_2PbI_4$ ($PhEPbI_4$) perovskite crystals directly from room temperature. We found that the perovskite crystals exhibit strong photoluminescence upconversion and near unity external quantum efficiency, properties that are responsible for the realization of net laser cooling. Our findings indicate that solution-processed perovskite thin films may be a highly suitable candidate for constructing integrated optical cooler devices.

Since optical refrigeration by anti-Stoke fluorescence was first predicted[1], most experimental demonstrations were carried out in rare earth element-doped materials due to their suitable energy spacing and high fluorescence external quantum efficiency[2–6]. Direct bandgap semiconductors possess several advantages over rare earth-based materials, such as high absorption and lower achievable temperature down to the liquid helium temperature due to the distinct statistics of carriers[7,8]. In addition, semiconductor optical coolers could be readily integrated into other optoelectronic devices. The main obstacle that hindered the experimental observation of laser cooling in semiconductors for decades was the low luminescence extraction efficiency[9]. GaAs, for instance, requires a minimum extraction efficiency of 20–30% at the optimal carrier density, which is difficult to achieve due to its large refractive index[8,9]. The recent successful laser cooling of 40 K on single a CdS nanobelt is an exception, in part due to a near-unity external quantum efficiency of the subwavelength thickness (~100 nm), in which photon trapping and re-absorption is no longer an issue[10]. Therefore, it is critical to find a suitable material with a high external quantum efficiency even in the bulk form to realize net laser cooling for practical applications.

Lead halide perovskites have garnered tremendous attention in the past few years due to their high performance as light absorbers in solar cells[11–14] and optically pumped lasers[15–17]. Recent work also shows that perovskite single crystals possess low trap-state density[18,19] and high external quantum efficiency[20], both of which are advantageous for laser cooling if a sufficient photoluminescence (PL) upconversion could be achieved. Interestingly, indeed we find that lead halide perovskite crystals in both 3D ($MAPbI_3$) and 2D ($PhEPbI_4$) forms show strong PL upconversion, suggesting the possibility of laser cooling. In this work, we demonstrate experimentally that $MAPbI_3$ platelets grown by vapour phase synthesis and $PhEPbI_4$ samples exfoliated from a bulk crystal by solution synthesis can be laser cooled by ~23.0 and 58.7 K, respectively, from room temperature.

Growth and optical properties of lead halide perovskites

Figure 1a shows an optical image of $MAPbI_3$ perovskite crystals with a platelet morphology on muscovite mica substrates prepared by a chemical vapour deposition (CVD) approach[21] (Methods and Supplementary Information Part 1.1 and Supplementary Fig. 1). The crystalline platelets are tens of micrometres in size, with a thickness varying from tens of nanometres to a few micrometres. The color difference of crystals originates from their optical interference difference depending on thickness, which can be accurately determined by atomic force microscopy (AFM) and profilometry (inset to Fig. 1a). The perovskite platelet crystals synthesized by this method exhibit good crystallinity with a tetragonal phase at room temperature[21] and a much better stability under laser illumination compared with the polycrystalline thin films that are usually obtained in solution spin-casting. Figure 1b shows an optical image of a thin film of $PhEPbI_4$ exfoliated from a solution-grown millimetre-sized crystal (inset to Fig. 1b) (Supplementary Information Part 1.2). Owing to the layered structure of $PhEPbI_4$, it can be readily exfoliated using the Scotch tape method, which provides samples with a suitable thickness for the cooling experiment. Figure 1c,d are the X-ray diffraction (XRD) patterns measured for as-grown $MAPbI_3$ platelets and $PhEPbI_4$ crystals, respectively. The layered structure of 2D $PhEPbI_4$ perovskites can also be seen from the XRD pattern with the periodic (002) plane peaks (Fig. 1d).

Figure 2a,d shows the temperature-dependent PL spectra of $MAPbI_3$ and $PhEPbI_4$, respectively from 77 to 340 K, excited by a 671 nm laser for $MAPbI_3$ and 473 nm laser for $PhEPbI_4$ with a low power excitation (that is, 5–15 μW) to minimize the heating effect. It is known that $MAPbI_3$ has an orthorhombic-to-tetragonal phase transition at ~150 K[22]. Our experimental results show that below 120 K, the PL peak at ~750 nm can be assigned to orthorhombic phase. From 120 to 160 K, the perovskite exhibits a phase transition that leads to the appearance of a lower energy peak at ~780 nm (dashed box), which corresponds to the tetragonal phase. From 160 to 340 K, as temperature increases the PL peak

[1]Division of Physics and Applied Physics, School of Physical and Mathematical Sciences, Nanyang Technological University, Singapore 637371, Singapore. [2]NOVITAS, Nanoelectronics Centre of Excellence, School of Electrical and Electronic Engineering, Nanyang Technological University, Singapore 639798, Singapore. †Present address: State Key Laboratory for Superlattices and Microstructures, Institute of Semiconductors, Chinese Academy of Sciences, Beijing 100083, China. *e-mail: qihua@ntu.edu.sg

© 2016 Macmillan Publishers Limited. All rights reserved

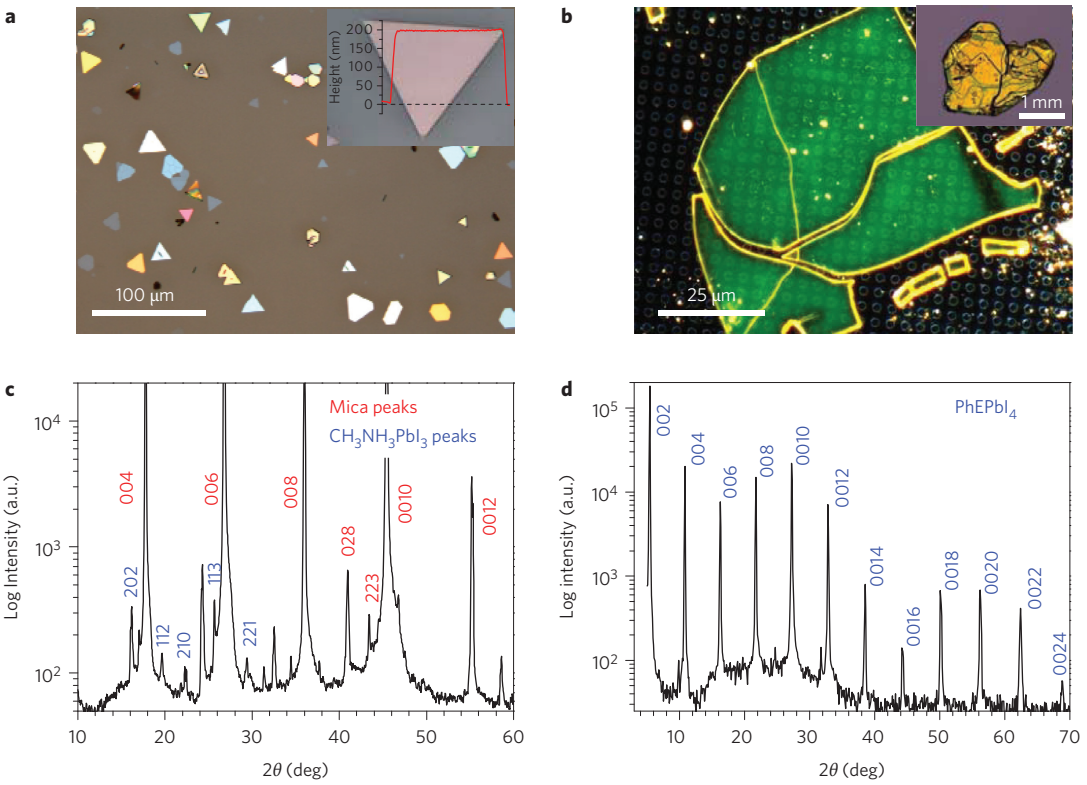

Figure 1 | Morphology and structural characterization of 3D and 2D perovskites. a, Optical image of as-grown $CH_3NH_3PbI_3$ 3D perovskite platelets on a muscovite mica substrate. Inset, an individual perovskite platelet with the AFM height profile. **b**, Optical image of exfoliated $PhEPbI_4$ 2D perovskite on a hole-patterned silicon substrate used for laser cooling experiments. Inset, millimetre-size 2D perovskite crystal grown from solution. **c**,**d**, XRD diffraction patterns of as-grown 3D and 2D perovskites, respectively.

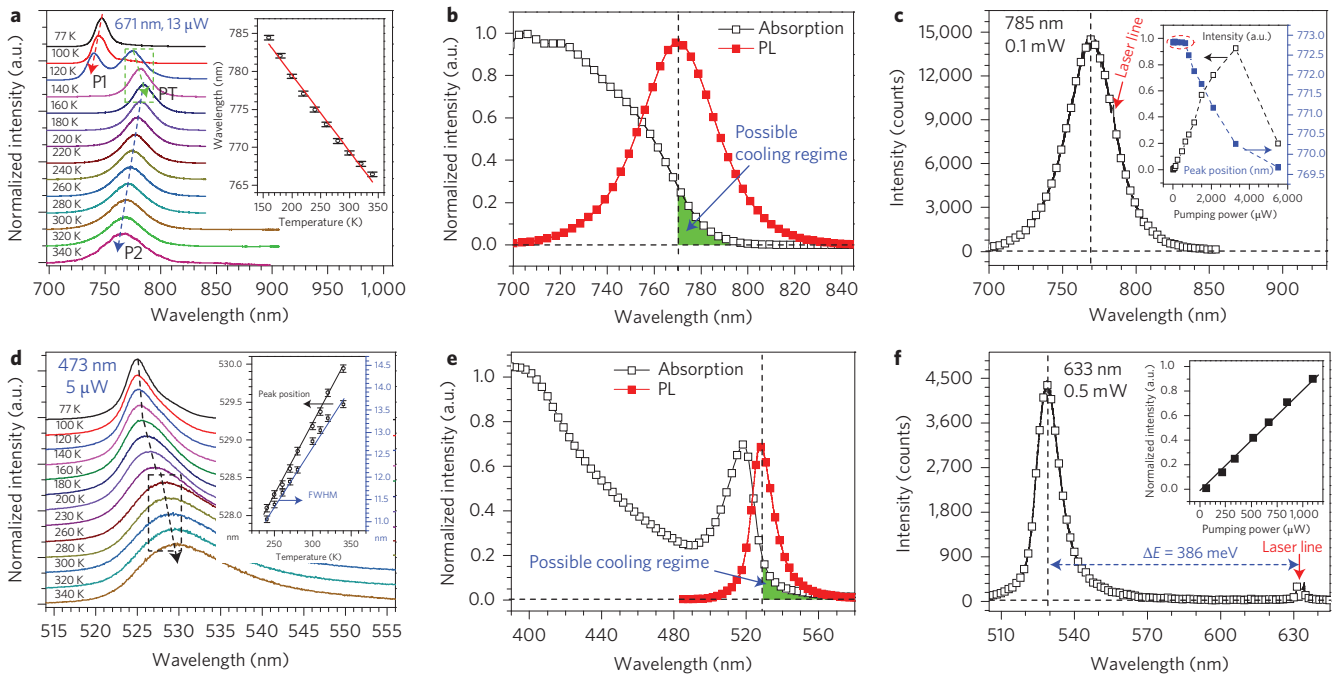

Figure 2 | Optical characterization of 3D and 2D perovskites. 3D (2D) perovskites are shown in **a**–**c** (**d**–**f**) respectively. (**a**, **d**): Normalized PL from 77 to 340 K. The inset is a temperature calibration curve extracted from temperature dependent PL data within the laser cooling experiment windows. (**b**, **e**): PL and the absorption spectra at 296 K. The green areas indicate possible cooling regime. (**c**, **f**): ASPL spectra at 296 K. The inset to (**c**) displays the peak position and ASPL intensity versus pump power. Below certain power (i.e. 1 mW), the intensity scales linearly with power indicating a phonon-assisted upconversion, and the peak position is stable (dash-line oval). Beyond that critical power, the photoluminescence peak blue-shifts indicating sample heating due to reabsorption and/or background absorption effect, although the ASPL still scales linearly until a slightly higher power (~3 mW). In 2D samples the pump power is limited within 1 mW constrained by the laser, which is in the linear regime (inset to **f**).

© 2016 Macmillan Publishers Limited. All rights reserved

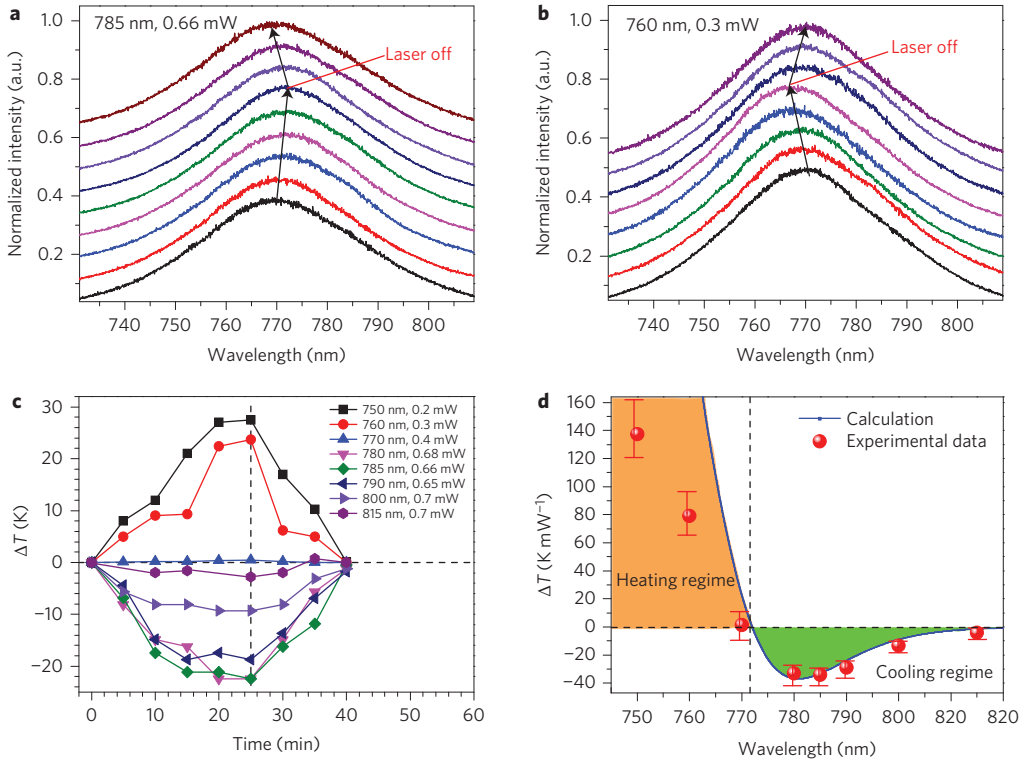

Figure 3 | Net laser cooling observations for 3D perovskite $CH_3NH_3PbI_3$. a, Evolution of PPLT spectra starting from 296 K, pumped by a 785 nm laser with a power of 0.66 mW. **b**, Evolution of PPLT spectra starting from 290 K, pumped by a 760 nm laser with a power of 0.3 mW. **c**, Temperature change versus time pumped by eight laser lines (815, 800, 790, 785, 780, 770, 760, and 750 nm), using data extracted from the PPLT spectra. **d**, Summary of measured maximum ΔT (red filled-circles) and theoretically calculated temperature change (blue curve) normalized to pump power for different pump wavelengths at 296 K.

linearly blueshifts as illustrated in the inset to Fig. 2a. Based on this relationship, a temperature calibration curve can be obtained relative to the band edge emission at room temperature. It is important to note that the PL shift of the 3D perovskite is in the opposite direction to conventional semiconductors, which will need further investigation for this material. A similar temperature calibration curve was also obtained for the 2D perovskite, as shown in Fig. 2d. Opposite to 3D perovskite, we note that the optical gap of 2D perovskite has similar trend versus temperature as traditional semiconductors. Figure 2b,e displays the Stokes PL (red curve) taken at 296 K and the corresponding absorption spectra measured from the same crystal (black curve)[23] for 3D and 2D perovskite, respectively. The PL peaks of 3D and 2D perovskites are at ~770 and 529 nm, respectively, in good agreement with other reports[24–27]. Towards the band tail the absorption decreases and reaches zero, indicating that there should be no substantial phonon-assisted upconversion PL beyond this wavelength. The green area under the absorption curve indicates a possible cooling regime where the excitation photon energy is less than that of mean emission PL. Next, we investigate the intensity of the anti-Stokes PL (ASPL) versus laser power (Fig. 2c,f). As shown in the inset of Fig. 2c for 3D case, below a certain excitation power, the ASPL intensity linearly depends on laser power, indicating that phonon-assisted up-conversion process dominates. Above this power, ASPL intensity deviates from the linear dependence and even decreases if the laser irradiation is sustained for a while, due to possible degradation at a high laser power (Supplementary Information Part 2). The blueshift of the ASPL peak above that critical power (inset to Fig. 2c) indicates the heating of the sample at higher excitation power (according to the calibration curve shown in Fig. 2a). Therefore, in our laser cooling experiment, we limit the excitation power to around 0.7 mW, which is below the critical power to prevent heating of sample. We should comment that this upper-bound value of the laser power varies from sample to sample, possibly due to variations in the crystalline quality and purity of the samples. Further improvement in sample quality may improve critical power and thus laser cooling performance. As shown in Fig. 2f for 2D perovskite, even at the excitation energy of 386 meV lower than the bandgap, the ASPL of 2D perovskite was still exceptionally strong. The power dependence ASPL (inset to Fig. 2f) also indicates that the upconversion is a phonon-assisted process, which is essential for realization of laser cooling in this material.

Laser cooling observation in 3D perovskite platelets

To measure the cooling effect of the crystals, we adopt the pump–probe luminescence thermometry (PPLT) technique previously used in rare earth materials and semiconductors[28] (Methods and Supplementary Information, Part 3 and Supplementary Figs 3, 4). The mica substrate (less than 100 μm) with perovskite crystals was suspended to isolate the sample from the copper cold finger of the cryostat. Mica exhibits excellent transparency (>95% for a 100 μm-thick film at 770 nm)[29,30], a low refractive index (~1.6) and low thermal conductivity (~0.45 $W\,m^{-1}\,K^{-1}$)[31]. Therefore, this design will reduce the background absorption, increase the luminescence extraction efficiency and reduce the thermal load during the cooling experiment. Figure 3a,b displays the evolution of the PL spectra for two representative cooling and heating cycles pumped at 785 and 760 nm, respectively. It is clearly seen that the PL redshifts when pumped by 785 nm, indicating a cooling process in the perovskite platelet (refer to the calibration curve shown in the inset to Fig. 2a). On the contrary, 760 nm pumping leads to a blueshifted band edge, indicating a heating process. After the pump lasers were turned off, the PL spectra returned to their original position, indicating that the cooling–warming cycle is reversible. A summary of a series of cooling and heating experiments with different pumping wavelengths is shown in Fig. 3c, whereas the full

© 2016 Macmillan Publishers Limited. All rights reserved

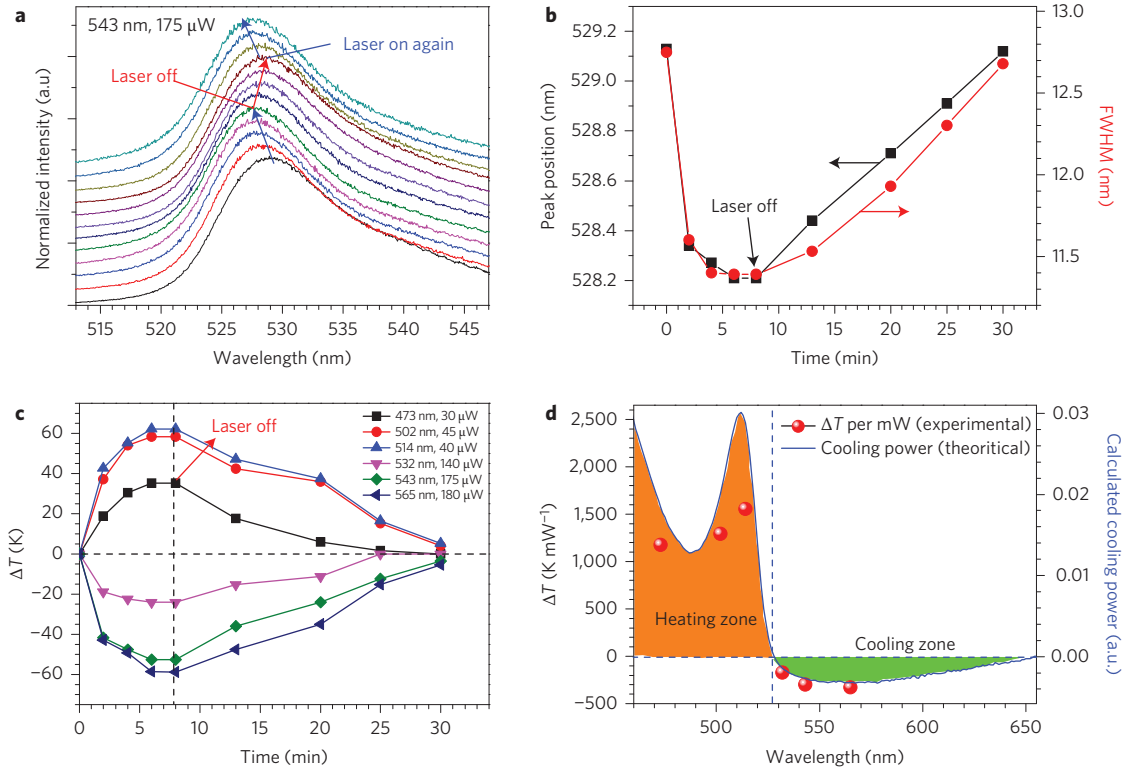

Figure 4 | Net laser cooling observations for 2D perovskite $(C_6H_5C_2H_5NH_3)_2PbI_4$. a, Evolution of PPLT spectra starting from 296 K, pumped by a 543 nm laser. The pump laser was turned on again to show that the cooling and warming processes were fully reversible. **b**, The peak position and FWHM extracted from PPLT spectra during laser cooling and warming processes show that both of them follow the temperature calibration curve in Fig. 2d inset. **c**, Temperature change versus time pumped by six lasers (473, 502, 514, 532, 543, and 565 nm), using data extracted from the PPLT spectra. **d**, Summary of measured maximum ΔT (red-filled-circles) and theoretically calculated temperature change (blue curve) normalized to pump power for different pump wavelengths at 296 K.

spectra for various temperatures are shown in the Supplementary Information (Supplementary Fig. 6). The data show that the perovskite platelet crystals could be cooled by a maximum of ~23.0 K from room temperature when pumped by 785 nm with a power of 0.66 mW. The normalized cooling power density (in K mW^{-1}) is plotted in Fig. 3d, showing a maximum cooling effect ~35.0 K mW^{-1} around 780–785 nm, which is much larger than in CdS nanobelts[10]. One possible explanation for such a big difference is the low thermal conductivity of perovskite materials[32]. The solid curve is a theoretical calculation based on the Sheik Bahae–Epstein (SB–E) theory, showing a reasonable agreement except for the heating data points (at 750 and 760 nm).

Laser cooling observation in 2D perovskite

Similar cooling experiments were carried out for 2D perovskite and the results are summarized in Fig. 4. Figure 4a shows the PPLT spectra of cooling–warming–cooling cycle starting from 296 K pumped by 543 nm laser. As we can see, whenever the pumping laser was on, the PPLT spectrum was blueshifted, indicating cooling of the crystal. This experiment shows that the cooling and warming process is reversible and also reproducible. Figure 4b shows the evolution of PL peak and full width at half maximum (FWHM) of the spectra extracted from Fig. 4a for the first cooling–warming cycle. It is noted that both the PL peak position and FWHM evolutions are in good agreement with the calibration curve shown in Fig. 2d for the 2D perovskite. This is strong evidence that the sample is indeed cooled down by the pump laser. Figure 4c, d summarizes the cooling and heating of the 2D perovskite crystal by various wavelength laser pumping. The maximum cooling of 58.7 K directly from room temperature was achieved with 565 nm laser excitation. The cooling and heating results also agree well with the calculation based on SB–E theory as shown in Fig. 4d.

To further elaborate the cooling of the 2D perovskite crystal, we designed a macroscopic optical cooler using the 2D perovskite crystal to cool an external thermal load of the CdSe nanobelts, reminiscent of a microscopic CdS solid-state optical cooler[33]. The experimental setup is schematically shown in Fig. 5a. A CdSe nanobelt grown by CVD was used as a temperature probe (and hence thermal load) for the cooling experiment. The nanobelts, with a thickness of ~100 nm, width of 2–4 μm, and length of ~10 μm, were placed on top of a mechanically exfoliated 2D perovskite crystal sheet (inset to Fig. 5a) that is supported by two SiO_2 bars for thermal isolation. The whole setup was placed inside a cryostat, which was then pumped down to 10^{-6} Torr to prevent environmental thermal conduction. In this experiment we used only one laser (that is, 543 nm) to pump 2D perovskite to induce laser cooling, while simultaneously the same laser is used to probe the PL of the CdSe nanobelt, which has a peak position around 710 nm as a temperature indicator. The temperature calibration curve extracted from the temperature-dependent PL for the CdSe nanobelt was done separately (Supplementary Information, Part 3 and Supplementary Fig. 5). The laser spot was positioned near the edge of the nanobelt so that the cooling of the CdSe nanobelt by the 2D perovskite crystal is maximized. The PPLT spectra evolution of the CdSe nanobelt during the cooling experiment is shown in Fig. 5b. Based on the temperature calibration curve (Supplementary Fig. 5), the CdSe nanobelt was observed to be cooled by ~28.0 K from room temperature. It is noted that the cooling result for the CdSe nanobelt is lower than the 2D perovskite itself as shown in Fig. 4a,c (which is ~52 K) for the same excitation

© 2016 Macmillan Publishers Limited. All rights reserved

condition. This is probably in part due to the heating effect caused by the absorption of the 543 nm wavelength by the CdSe nanobelt, as well as the thermal conductive loss due to the nanobelt.

Laser cooling origin in perovskite

To understand the excellent laser cooling properties of the perovskite crystals, we turn to the SB–E theory[8], which describes the net cooling power P_{net} in the semiconductor as:

$$P_{net} = \eta_e BN^2(h\nu - h\bar{\nu}_f) + ANh\nu + CN^3 h\nu + \Delta P \quad (1)$$

where η_e is the extraction efficiency of the PL, N is the photo-excited electron–hole carrier density; A, B and C are the recombination coefficients of nonradiative (one particle), radiative (two particle), and Auger (three particle) processes, respectively; ν and $\bar{\nu}_f$ are excitation and mean emission luminescence photon frequency, respectively; and ΔP is a residual heating term accounting for free-carrier absorption and other parasitic absorptive processes, $\Delta P = \alpha_b I + \sigma_{fca} NI$, where α_b is the background absorption, σ_{fca} is the free-carrier absorption cross-section and I is the laser irradiance intensity. This model excludes any possible two-photon process, which usually releases extra energy into lattice heat. When the excitation occurs near the band-edge, the interband absorption dominates and thus the term ΔP can be ignored. Then, the cooling efficiency could be expressed as:

$$\eta_c = \eta_{ext}\frac{\bar{\nu}_f}{\nu} - 1 = \left(\frac{\eta_e BN^2}{AN + \eta_e BN^2 + CN^3}\right)\frac{\bar{\nu}_f}{\nu} - 1 \quad (2)$$

here, $\eta_{ext} = \eta_e BN^2/(AN + \eta_e BN^2 + CN^3)$, representing the external quantum efficiency. Cooling is possible when η_c is positive. The above phenomenological theory considers only the free electron model, more discussions that include the excitonic effect, band-tail states and surface plasmon-assisted laser cooling can be found in the literature[34–37].

Based on equation (2), we plot the cooling efficiency as a function of external quantum efficiency η_{ext} and $\Delta E = h\bar{\nu}_f - h\nu$ for $MAPbI_3$ (band edge of 770 nm) shown in Fig. 6a. As can be seen from Fig. 6a, a minimal η_{ext} of ~0.95 and ~0.99 are required for excitation at 815 nm (ΔE = 95 meV) and 780 nm (ΔE = 20 meV), respectively, as indicated by the dashed lines. The cooling efficiency increases as η_{ext} approaches unity. The calculation is valid only when the background and free-carrier absorption are negligible. As the excitation photon energy moves into the Urbach tail (that is, large ΔE), the interband absorption reduces dramatically and thus the background and free-carrier absorption are no longer negligible.

We then determine η_{ext} for the perovskite platelets by using a bolometric calibration method that has been described in the literature to measure external quantum efficiency of GaAs[7,38]. The experimental setup is similar to our laser cooling experiment described above. We used various laser wavelengths with energies higher than that of the mean emission PL of the perovskite platelets to pump and record the temperature change in the samples. The excitation power for different wavelengths was adjusted so that the emission PL intensity in each experiment is comparable. This is to ensure that the total emitted photons for each wavelength are constant if the PL collection efficiency of our optical system remained unchanged in all measurements. In addition, the excitation powers should be kept low enough (<0.1 mW) to avoid heating of the sample, which may affect the local temperature. Figure 6b shows the fractional heating at various wavelength excitations for four different thicknesses. From these results, we can determine λ_{cr}, which is the intersection between the linear fit of the fractional heating at different wavelengths and the x axis. This was then used to calculate η_{ext} for the perovskite platelets as shown in Fig. 6c. As we can see, η_{ext} is extremely high for those perovskite platelets and reaches maximum at thicknesses of around 1.5 μm. This high value of η_{ext} (~99.8%) explains why we could observe net laser

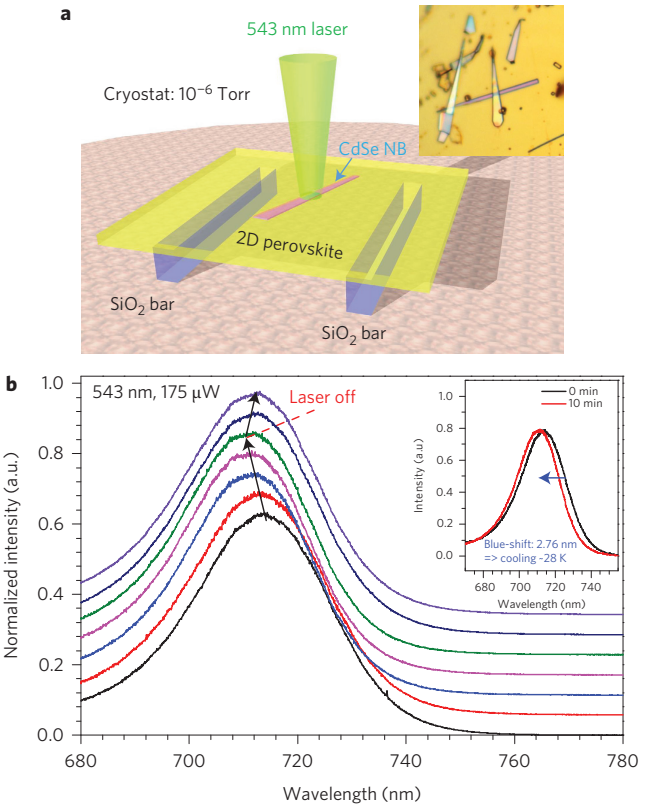

Figure 5 | A macroscopic 2D perovskite optical cooler cooling a CdSe nanobelt thermal load. a, Experimental setup. A CdSe nanobelt with a thickness of ~100 nm, width of ~2–4 μm and length of ~10 μm was placed on top of an exfoliated 2D perovskite sample. The 543 nm pump laser was used to excite the 2D perovskite area near the nanobelt. Inset, an optical image of the CdSe nanobelts laid on top of the 2D perovskite sample. **b**, Evolution of PPLT spectra starting from 296 K, which show a blue-shift of 2.76 nm after 10 min pumping indicating a cooling of 28 K (inset).

cooling even with the excitation wavelength at 780 nm where the minimal η_{ext} required for cooling is 99% (Fig. 6a).

To further elaborate on this, we conducted thickness-dependent cooling experiments on a variety of platelet crystals (Supplementary Information, part 5). Figure 6d summarizes the thickness dependent ΔE (upper panel), calculated cooling efficiency (middle panel) and calculated cooling power by 785 nm excitation (lower panel). The cooling power of perovskite platelets with different thicknesses was estimated based on the actual absorption measured. We note that the trend of the calculated cooling power versus thickness agrees with the experimental values in K mW^{-1}. The maximal cooling of 8.8 μW can be achieved at a thickness of ~2.0 μm, in agreement with our experimental observation (Supplementary Information, Part 5, 6 and Supplementary Fig. 8). The estimated blackbody radiation is ~2.0 nW, therefore the thermal conductive heat dissipation dominates. Similar laser cooling measurements were conducted on solution-processed thin crystals on mica (Supplementary Information, Part 7 and Supplementary Fig. 9). The result shows that a net cooling of ~20 K can be readily obtained, which opens up the possibility of scaling up the material synthesis towards a practical optical refrigeration device. It is important to note that polycrystalline thin films prepared by the spin-casting method cannot tolerate similar pump power, which leads to rapid degradation of the films. Furthermore, we have observed that a few other halide compounds in the perovskite family $CH_3NH_3PbX_3$ (X= Cl, Br, I, and their combinations) show strong upconversion PL (Supplementary Information, Part 8 and

© 2016 Macmillan Publishers Limited. All rights reserved

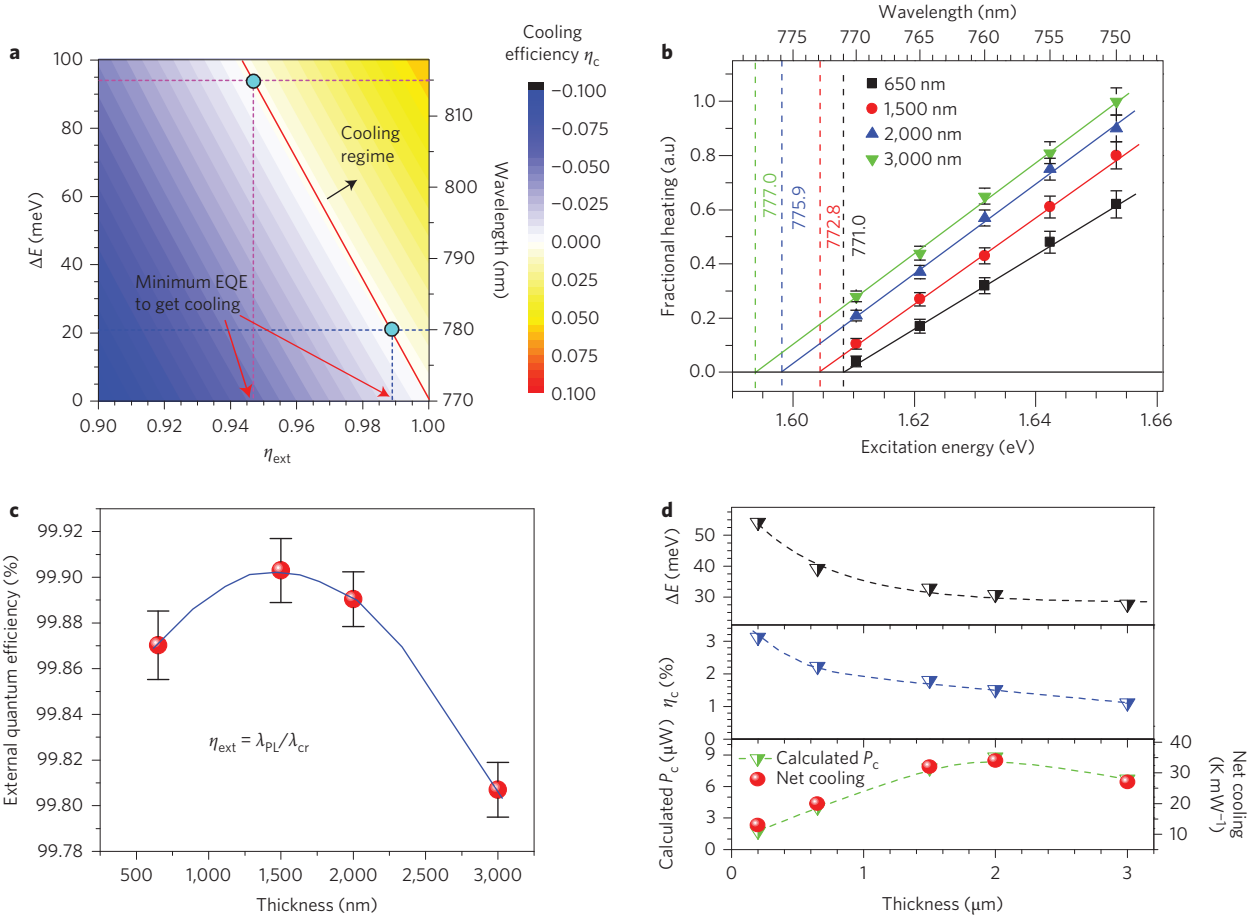

Figure 6 | Condition for laser cooling in $CH_3NH_3PbI_3$ platelets. a, Calculated cooling efficiency as a function of external quantum efficiency and energy difference between the excitation photon and emission photon energies **b**, Fractional heating (normalized with excitation power and absorption at the wavelength) for different sample thicknesses excited at higher bandgap wavelengths (750, 755, 760, 765 and 770 nm). The cross-wavelength (λ_{cr}), which is the intersection between linear fitting line of fractional heating data and the *x* axis at 0 fractional heating, is used to calculate external quantum efficiency. **c**, External quantum efficiency of the perovskite platelets with different thicknesses calculated from (**b**). **d**, Thickness dependence of the energy difference (upper), cooling efficiency (middle), and calculated cooling power (lower). The calculated cooling powers for different thicknesses are in good agreement with experimental results for net cooling (red filled-circle).

Supplementary Fig. 10), which suggests considerable promise in expanding the laser cooling arsenal, and for the optimizing and accomplishing higher net cooling in those materials.

Conclusions

We have demonstrated laser cooling of both 2D and 3D lead halide perovskite materials. The maximum cooling of 23.0 and 58.7 K has been achieved for the $MAPbI_3$ and $PhEPbI_4$ perovskites, respectively. We have also demonstrated an actual perovskite optical cooler in which a CdSe nanobelt can be cooled by 28.0 K from room temperature. Our work expands the toolbox for optical refrigeration extensively, considering the numerous combinations of inorganic-organic perovskites. With the facile solution processing and accessible crystallization temperature of these perovskite materials, our work opens up the possibility of laser cooling devices that are easily bonded to electronic and optoelectronic thermal loads. The remaining challenges are to scale up the current vapour phase or solution synthesis towards a uniform macroscale crystalline film and the proper design of the heat sink, as the thermal conductivity of those perovskites is usually low.

Methods

Methods and any associated references are available in the online version of the paper.

Received 13 August 2015; accepted 6 November 2015; published online 21 December 2015

References

1. Pringsheim, P. Zwei bemerkungen über den unterschied von lumineszenz- und temperaturestrahlung. *Z. Phys. A* **57,** 739–746 (1929).
2. Epstein, R. I., Buchwald, M. I., Edwards, B. C., Gosnell, T. R. & Mungan, C. E. Observation of laser-induced fluorescent cooling of solid. *Nature* **377,** 500–503 (1995).
3. Gosnell, T. R. Laser cooling of a solid by 65K starting from room temperature. *Opt. Lett.* **24,** 1041–1043 (1999).
4. Melgaard, S., Seletskiy, D., Albrecht, A. & Sheik-Bahae, M. First solid-state cooling below 100K. *SPIE Newsroom* (13 March 2015).
5. Seletskiy, D. V. *et al.* Laser cooling of solids to cryogenic temperatures. *Nature Photon.* **4,** 161–164 (2010).
6. Seletskiy, D. V. *et al.* Local laser cooling of Yb:YLF to 110 K. *Opt. Express* **19,** 18229–18236 (2011).
7. Gauck, H., Gfroerer, T. H., Renn, M. J., Cornell, E. A. & Bertness, K. A. External radiative quantum efficiency of 96% from a GaAs/GaInP heterostructure. *Appl. Phys. A* **64,** 143–147 (1997).
8. Sheik-Bahae, M. & Epstein, R. I. Can laser light cool semiconductors? *Phys. Rev. Lett.* **92,** 247403 (2004).
9. Sheik-Bahae, M. & Epstein, R. I. Optical refrigeration. *Nature Photon.* **1,** 693–699 (2007).
10. Zhang, J., Li, D., Chen, R. & Xiong, Q. H. Laser cooling of a semiconductor by 40 Kelvin. *Nature* **493,** 504–508 (2013).
11. Burschka, J. *et al.* Sequential deposition as a route to high-performance perovskite-sensitized solar cells. *Nature* **499,** 316–319 (2013).

© 2016 Macmillan Publishers Limited. All rights reserved

12. Lee, M. M., Teuscher, J., Miyasaka, T., Murakami, T. N. & Snaith, H. J. Efficient hybrid solar cells based on meso-superstructured organometal halide perovskites. *Science* **338,** 643–647 (2012).
13. Stranks, S. D. *et al.* Electron-hole diffusion lengths exceeding 1 micrometer in an organometal trihalide perovskite absorber. *Science* **342,** 341–344 (2013).
14. Xing, G. *et al.* Long-range balanced electron- and hole-transport lengths in organic-inorganic $CH_3NH_3PbI_3$. *Science* **342,** 344–347 (2013).
15. Xing, G. *et al.* Low-temperature solution-processed wavelength-tunable perovskites for lasing. *Nature Mater.* **13,** 476–480 (2014).
16. Zhang, Q., Ha, S. T., Liu, X. F., Sum, T. C. & Xiong, Q. H. Room-temperature near-infrared high-q perovskite whispering-gallery planar nanolasers. *Nano Lett.* **14,** 5995–6001 (2014).
17. Xing, J. *et al.* Vapor phase synthesis of organometal halide perovskite nanowires for tunable room-temperature nanolasers. *Nano Lett.* **15,** 4571–4577 (2015).
18. Dong, Q. *et al.* Solar cells. Electron-hole diffusion lengths >175 μm in solution-grown $CH_3NH_3PbI_3$ single crystals. *Science* **347,** 967–970 (2015).
19. Shi, D. *et al.* Solar cells. Low trap-state density and long carrier diffusion in organolead trihalide perovskite single crystals. *Science* **347,** 519–522 (2015).
20. Wehrenfennig, C., Eperon, G. E., Johnston, M. B., Snaith, H. J. & Herz, L. M. High charge carrier mobilities and lifetimes in organolead trihalide perovskites. *Adv. Mater.* **26,** 1584–1589 (2014).
21. Ha, S. T. *et al.* Synthesis of organic-inorganic lead halide perovskite nanoplatelets: Towards high performance perovskite solar cells and opto-electronic devices. *Adv. Opt. Mater.* **2,** 838–844 (2014).
22. Baikie, T. *et al.* Synthesis and crystal chemistry of the hybrid perovskite $(CH_3NH_3)PbI_3$ for solid-state sensitised solar cell applications. *J. Mater. Chem. A* **1,** 5628–5641 (2013).
23. Roosbroeck, W. V. & Shockley, W. Photon-radiative recombination of electrons and holes in germanium. *Phys. Rev.* **94,** (1954).
24. Mosconi, E., Amat, A., Nazeeruddin, M. K., Grätzel, M. & De Angelis, F. First-principles modeling of mixed halide organometal perovskites for photovoltaic applications. *J. Phys. Chem. C* **117,** 13902–13913 (2013).
25. Stoumpos, C. C., Malliakas, C. D. & Kanatzidis, M. G. Semiconducting tin and lead iodide perovskites with organic cations: phase transitions, high mobilities, and near-infrared photoluminescent properties. *Inorg. Chem.* **52,** 9019–9038 (2013).
26. Kitazawa, N. & Watanabe, Y. Optical properties of natural quantum-well compounds $(C_6H_5\text{-}C_nH_{2n}\text{-}NH_3)_2PbBr_4$ (n=1–4). *J. Phys. Chem. Solids* **71,** 797–802 (2010).
27. Lanty, G. *et al.* Room-temperature optical tunability and inhomogeneous broadening in 2D-layered organic-inorganic perovskite pseudobinary alloys. *J. Phys. Chem. Lett.* **5,** 3958–3963 (2014).
28. Imangholi, B. *et al.* Differential luminescence thermometry in semiconductor laser cooling. *Proc. SPIE* **6115,** 61151C (2006).
29. Chen, R. *et al.* Excitonic properties and near-infrared coherent random lasing in vertically aligned CdSe nanowires. *Adv. Mater.* **23,** 1404–1408 (2011).
30. Utama, M. I. *et al.* Vertically aligned cadmium chalcogenide nanowire arrays on muscovite mica: a demonstration of epitaxial growth strategy. *Nano Lett.* **11,** 3051–3057 (2011).
31. Gray, A. S. & Uher, C. Thermal conductivity of mica at low temperatures. *J. Mater. Sci.* **12,** 959–965 (1977).
32. Pisoni, A. *et al.* Ultra-low thermal conductivity in organic-inorganic hybrid perovskite $CH_3NH_3PbI_3$. *J Phys Chem Lett* **5,** 2488–2492 (2014).
33. Li, D., Zhang, J., Wang, X., Huang, B. & Xiong, Q. H. Solid-state semiconductor optical cryocooler based on CdS nanobelts. *Nano Lett.* **14,** 4724–4728 (2014).
34. Khurgin, J. B. Band gap engineering for laser cooling of semiconductors. *J. Appl. Phys.* **100,** 113116 (2006).
35. Khurgin, J. B. Surface plasmon-assisted laser cooling of solids. *Phys. Rev. Lett.* **98,** 177401 (2007).
36. Khurgin, J. B. Role of bandtail states in laser cooling of semiconductors. *Phys. Rev. B* **77,** 235206 (2008).
37. Rupper, G., Kwong, N. H. & Binder, R. Large excitonic enhancement of optical refrigeration in semiconductors. *Phys. Rev. Lett.* **97,** 117401 (2006).
38. Wang, C. G., Li, C. Y., Hasselbeck, M. P., Imangholi, B. & Sheik-Bahae, M. Precision, all-optical measurement of external quantum efficiency in semiconductors. *J. Appl. Phys.* **109**, 093108 (2011).

Acknowledgements

Q.X. gratefully acknowledges the strong support of this work from Singapore National Research Foundation through an Investigatorship Award (NRF-NRFI2015–03), Ministry of Education via two AcRF Tier 2 grants (MOE2013-T2-1-049 and MOE2015-T2-1-047) and Tier1 grant (2013-T1-002-232). This work was also supported in part by AFOSR through its Asian Office of Aerospace Research and Development (FA2386-13-1-4112).

Author contributions

S.T.H. and Q.X. conceived the idea; S.T.H., C.S., J.Z., and Q.X. designed the experiments; S.T.H. and C.S. performed the experiments; S.T.H., C.S., J.Z., and Q.X. analysed the data and wrote the manuscript.

Additional information

Supplementary information is available in the online version of the paper. Reprints and permissions information is available online at www.nature.com/reprints. Correspondence and requests for materials should be addressed to Q.X.

Competing financial interests

The authors declare no competing financial interests.

© 2016 Macmillan Publishers Limited. All rights reserved

Methods

The 3D $MAPbI_3$ crystals were synthesized on a mica substrate using a home-built CVD system. The detailed synthesis and characterization have been published elsewhere[21]. The mica substrate with the grown perovskite platelet crystals was peeled off to a thickness below 100 μm and suspended over two silicon supports. The 2D $PhEPbI_4$ millimetre-sized crystals were grown by slowly evaporating saturated $PhEPbI_4$ solution in γ-butyrolactone. The crystals were then mechanically exfoliated by Scotch tape to the desired thickness and placed directly over two silicon supports. The whole samples were then mounted on the cold finger of a continuous flow microscopy cryostat. PPLT technique was used to cool and measure the local temperature variation of the perovskite platelets. The probe beams (671 nm for the 3D case, and 473 nm for the 2D case) were kept as low as 13 and 5 μW, respectively, to eliminate laser heating effects. Both pump (c.w. Ti-sapphire tunable wavelength laser from 750–850 nm for the 3D case; and solid states 502, 514, 532, 543, 565 nm for the 2D case) and probe beams were collimated and focused thorough a 50× objective onto specific local area on the perovskite crystals. All of the spectra were collected by a confocal triple grating spectrometer (Horiba-JY T64000) in a backscattering configuration. With a 640 mm focal length and 1,800 mm^{-1} grating, the highest spectral resolution is ~0.5 cm^{-1}, corresponding to ~0.01 nm around 500 nm. Full methods and more details can be found in the Supplementary Information.

© 2016 Macmillan Publishers Limited. All rights reserved